Influence of roughness and grinding direction on the thickness and adhesion of sol-gel coatings deposited by dip-coating on AZ31 magnesium substrates. A Landau-Levich equation revision

J.P. Fernández-Hernán[*], *A.J. López, B. Torres, J. Rams.*

Área de ciencia e ingeniería de materiales, ESCET, Universidad Rey Juan Carlos, C/ Tulipán, s/n, Móstoles 28933, Madrid, España.

ABSTRACT

AZ31 magnesium alloys with four different roughness values and two different grinding directions were coated with sol-gel silica coatings to assess the influence of the initial surface conditions of the substrates on the final coating thickness. Sol-gels were prepared from two silicon alkoxide precursors and deposited on the surface of the magnesium substrates by the dip-coating method. Roughness tester and scanning electron microscopy (SEM) were used to assess the thickness of the silica coatings and the presence of defects in the coatings. Shear stress tests were developed to study the adhesion of the coatings. An analysis of variance was carried out to determine the implication of the substrate roughness and the direction of the grinding lines in the final sol-gel coating thickness and its adhesion on the substrate. The results show that the roughness has a significant influence both on the thickness and on the adhesion of the coatings. Thus, thicker coatings were obtained on substrates with higher roughness values, going from 2.18 µm to 1.42 µm for substrate roughness values of 1.47 µm and 0.27 µm respectively, in the case of horizontal grinding lines, and from 2.01 µm to 1.37 µm for substrate roughness values of 1.47 µm and 0.27 µm respectively, in the case of vertical grinding lines. However, the grinding direction has no significant influence on the thickness nor the adhesion, but it has a clear influence on the formation of defects in the coatings. Finally, the inclusion of the *r* parameter in the Landau-Levich equation is proposed to adjust it, taking into account the roughness of the substrates intended to be coated and the evaporation of solvent and water from the coating during the dip-coating.

[*] *Corresponding author: Sr. Juan Pablo Fernández-Hernán;*
Tel.: +34 646 204 239; e-mail: juanpablo.fernandez@urjc.es

Keywords: Magnesium alloy; Roughness; Grinding direction; Sol-gel; Dip-coating; Coating thickness

1. Introduction

Magnesium and magnesium alloys are arousing interest in some fields as biomedical or automotive industries where these materials could be used for several applications due to their properties [1-7]. Magnesium is the lightest of the structural metals and has a resistance/weight ratio better than aluminium and steel. It has a low-density value and the lowest Young modulus among the metals used as biomaterials, close to that of natural bone. Moreover, magnesium is biocompatible, biodegradable, and an osteogenic material [8-10].

However, the major drawback of these materials is that magnesium is a very reactive metal and is prone to suffer from corrosion processes, which limits its use in the previously described fields. Some strategies are used to improve the corrosion resistance of the magnesium alloys such as surface modifications or the application of coatings on the surface of the magnesium substrate [11-16].

Concerning coatings, there are several technologies to create them, like high energy processes such as HVOF [17] or low energy methods as spin-coating, dip-coating, spray coating, etc. [18-22]. Among them, the dip-coating method has been widely used as it is simple and can be applied on pieces in a very wide range of sizes. The combination of the sol-gel synthesis with the dip-coating method has been deeply studied and used to generate micrometric ceramic coatings with different properties [23-31]. The sol-gel synthesis method allows mixing different metal alkoxide precursors to obtain hybrid coatings. In this method, the hydrolysis and polycondensation of the colloidal particles in the initial solution (sol), create a three-Dimensional network (gel) which, after the drying of the liquid phases inside the interconnected network and an aging process, becomes a solid ceramic material [32, 33]. Moreover, the sol-gel process allows the addition of different substances and nanoparticles, during the liquid synthesis, which can improve specific properties of the coatings like the adhesion on the substrate, the hardness and toughness, or provide the underlying substrate

with corrosion resistance, biocompatibility, or bactericide properties [34-38]. This way, coatings generated by sol-gel can be used to overcome the shortcomings of the substrates and to enlarge the fields where the substrate material can be used.

The dip-coating method consists of the immersion of the substrate that is intended to be coated in a dilution made of the material that is going to form the coating, and the subsequent extraction from the dilution with a controlled withdrawal speed. During the extraction, part of the coating material remains on the surface of the substrate creating a coating after the evaporation of the solvent of any other process that can take place in the thin layer. For Newtonian liquids, the thickness of this coating is a function of some properties of the fluid, i.e., surface tension, viscosity or density, as well as a function of the gravity and the withdrawal speed, as it is shown in equation 1, which is the Landau-Levich equation for Newtonian liquids [22][39, 40].

$$h = 0.94 \frac{(\eta \,.\, v)^{2/3}}{{\gamma_{LV}}^{1/6} (\rho \,.\, g)^{1/2}} \quad (1)$$

In this equation, η is the viscosity of the solution, v is the withdrawal speed from the solution, ρ is the density of the solution, g is the gravity acceleration and γ is the liquid-vapour surface tension.

Besides all of these parameters, the roughness of the substrate and the direction of the grinding lines with respect to the withdrawal direction during the dip-coating process can be important factors affecting the final thickness of the coatings. Several authors have studied how the roughness of the substrates intended to be coated affect different properties of the sol-gel coatings deposited on them [41- 44].

In this research, AZ31 magnesium alloy samples with four different roughness values and two grinding directions were studied to assess the influence of these parameters in the final thickness of sol-gel silica coatings deposited on their surfaces by the dip-coating method. Moreover, a new parameter was proposed to be included in the Landau-Levich equation to

adjust it with the roughness value of the coated substrate. This parameter also considers the effect of the evaporation of the liquid phases from the coating during the dip-coating method.

2. Materials & methods

2.1 Substrate material

The composition of the AZ31 magnesium alloy plates provided by Magnesium Elektron is shown in Table I. The plates were cut into 12×12×2.5 mm^3 samples. Before coating, all the samples were grounded with SiC grit papers. In this research, four different grinding finishing were tested. The samples were grounded using 120 SiC, 400 SiC, 800 SiC, and 1200 SiC grit paper sizes to obtain the four different grinding conditions. Finally, all the samples were ultrasonically cleaned by immersion in isopropanol for 10 minutes and air-dried.

Table I. AZ31B magnesium alloy composition in wt. %.

Al	Zn	Mn	Si	Ca	Fe	Ni	Cu	Mg
2.9	0.75	0.29	0.01	<0.005	0.004	0.0013	<0.0005	Bal.

2.2 Substrate roughness assessment

Before coating, the roughness of the magnesium substrates with different grinding conditions was assessed using a roughness tester (Surftest Mitutoyo SJ-210). Three different measurements were made for each grinding condition, for measuring the average roughness (*Ra*) and the root mean square (*Rq*) of the surfaces. The roughness corresponds with the average value measured along three different lines of 3.5 mm, perpendicular to the grinding direction, for each sample (ISO 4287:1997).

2.3 Coating generation and deposition

The coatings used in this research consisted of monolayer hybrid inorganic-organic silica films synthesized by the sol-gel method, from two silicon alkoxides, Tetraethyl Orthosilicate (TEOS; $Si(C_2H_5O)_4$) and Methyl-triethoxysilane (MTES; CH_3-$Si(C_2H_5O)_3$). These precursors were mixed in a magnetic stirrer for 10 minutes in a molar fraction of 40 % TEOS and 60 %

MTES. Then, isopropanol and 0.1 M HCl acidulated distilled water were added to the initial precursors mixture. The molar ratio between all the components was: 1 mol of 40 % TEOS / 60 % MTES mixture, 5 mols of isopropanol, and 10 mols of the acidulated distilled water, this ratio was optimized in previous research [11].

The final mixing was magnetically stirred for 2 hours at room temperature and then let stand for 30 minutes to let the hydrolysis and polycondensation reactions in the sol to be totally completed before coating. Figure 1 shows a diagram of the different steps in the sol-gel synthesis.

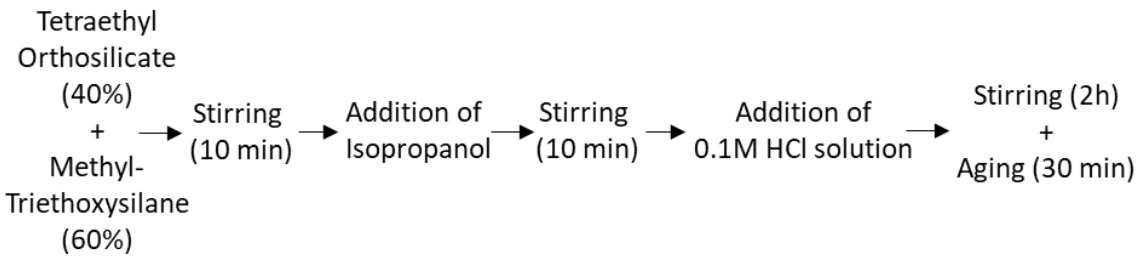

Figure 1. Diagram of the different steps in the sol-gel synthesis.

Once the sol was synthesized, the samples were coated by dip-coating. After immersing the samples in the sol for 1 minute, they were extracted from the sol with a controlled speed of 35 cm/min. This withdrawal speed was established in previous research, where homogeneous, compact, and crack-free coatings were obtained [11]. In this research, not only the influence of the roughness in the coating thickness was studied but the influence of the direction of the grinding lines in relation to the withdrawal direction during the dip-coating process. Thus, two different directions were studied as it can be seen in Figure 2. The withdrawal direction can be perpendicular to the grinding lines (horizontal lines, Figure 2a) or parallel to them (vertical lines, Figure 2b). These two conditions were assessed for each grit finishing. All the conditions evaluated in this research are shown in Table II.

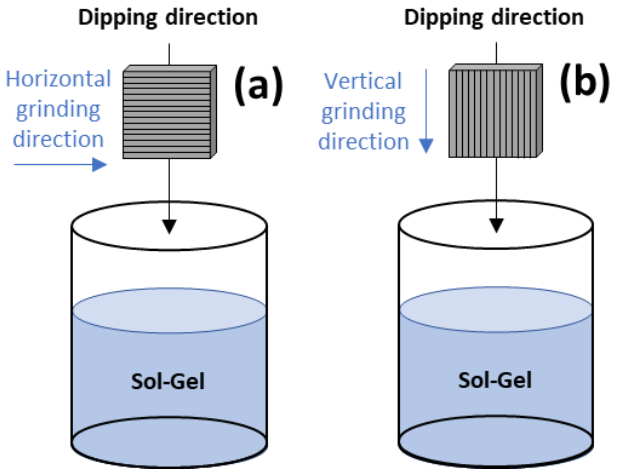

Figure 2. Scheme of the two different coating modes. (a) Horizontal grinding lines and perpendicular to withdrawal direction. (b) Vertical grinding lines and parallel to withdrawal direction.

Table II. Sample conditions.

Sample name	Grinding	Grinding lines
120 H	SiC 120 grit paper	Horizontal
400 H	SiC 400 grit paper	Horizontal
800 H	SiC 800 grit paper	Horizontal
1200 H	SiC 1200 grit paper	Horizontal
120 V	SiC 120 grit paper	Vertical
400 V	SiC 400 grit paper	Vertical
800 V	SiC 800 grit paper	Vertical
1200 V	SiC 1200 grit paper	Vertical

After the dip-coating, a heat treatment consisting of drying at 100 ºC for 24 hours followed by a sintering treatment at 200 ºC for 24 hours was applied as the final step.

2.4 Scanning electron microscopy

Once the samples were coated, scanning electron microscopy (SEM – HITACHI S3400N) was used to characterize the coatings on the different samples. Micrographs were taken with the samples tilted 60 º with respect to the horizontal plane inside the SEM to evaluate the thickness and the integrity of the coatings, looking for cracks and defects. Moreover, SEM was used to assess the surface of the substrates after the shear stress tests.

2.5 Hydrophobicity assessment

Before coating, contact angle tests were carried out by the sessile drop technique [45] and using a goniometer (RAMÉ-HART 200-F1). Distilled water droplets were deposited on the surface of the metallic substrates with different grinding conditions. Macrographs of the droplets were taken at 10 s, 30 s, and 60 s after the deposition, to evaluate the contact angle of water on the different AZ31 substrates.

2.6 Coating adhesion test

The adhesion of the coatings on the samples with the different grinding conditions was assessed by shear tests (Zwick / Roel type 8594.60 testing machine). 1 cm^2 of every coating was glued to an uncoated substrate (Figure 3) using the bi-component epoxy adhesive Loctite® EA 9466. In all cases, the orientation of the test was in the extraction direction. Therefore, the substrates with horizontal grinding lines were glued with the lines perpendicular to the shear stress direction. On the other hand, the samples with vertical grinding lines were glued with the lines parallel to the shear stress direction.

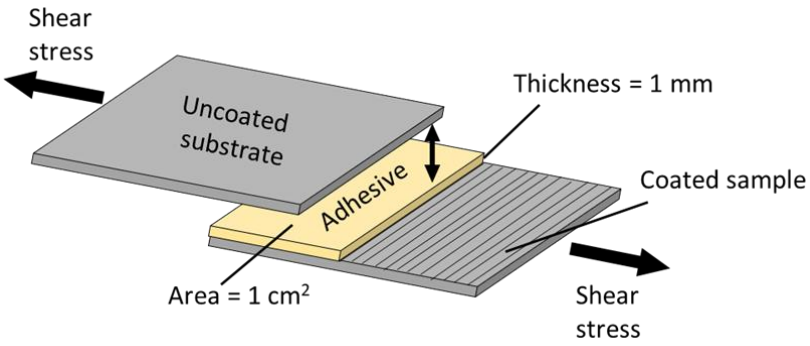

Figure 3. Scheme of the set-up used in the shear tests to evaluate the adhesion of the coatings.

2.7 Analysis of variance

Analysis of variance was carried out [46] to study the significance of the substrate roughness and the direction of the grinding lines used as factors on the values of coating thickness, which was the studied variable. The values obtained with this analysis were the combination of the squares (*SS*), the degrees of freedom (*DF*), the *F*-ratio (*F*), the probability of null hypothesis H_o (*p*), and the percentage contribution of each factor.

To assume the null hypothesis H_o means that the factor studied has no significance on the variable. To know if each factor has significance on the variable, the parameter *p* is used to accept or reject the null hypothesis. Thus, if $p < \alpha$, where $\alpha = 0.05$, then the null hypothesis can be rejected and the alternate hypothesis H_a, that the factor has a significance on the variable, can be accepted.

3. Results

3.1 Roughness

Figure 4 shows the different roughness parameters (*Ra*, *Rq*) for the AZ31 substrates treated with the four different SiC grit papers. As expected, lower roughness values were obtained on the surface of the AZ31 samples for the grit papers with the finer grain size. Moreover, the deviation values were also smaller for the lower roughness values, obtained using 800 and 1200 grit papers. Thus, the *Ra* values obtained for each grit paper were: 1.47 µm for 120 grit, 1.03 µm for 400 grit, 0.42 µm for 800 grit, and 0.27 µm for 1200 grit.

Rq values were slightly higher than *Ra* values indicating that the average amplitude from the mean line is higher than the average of peaks and valleys in the height direction.

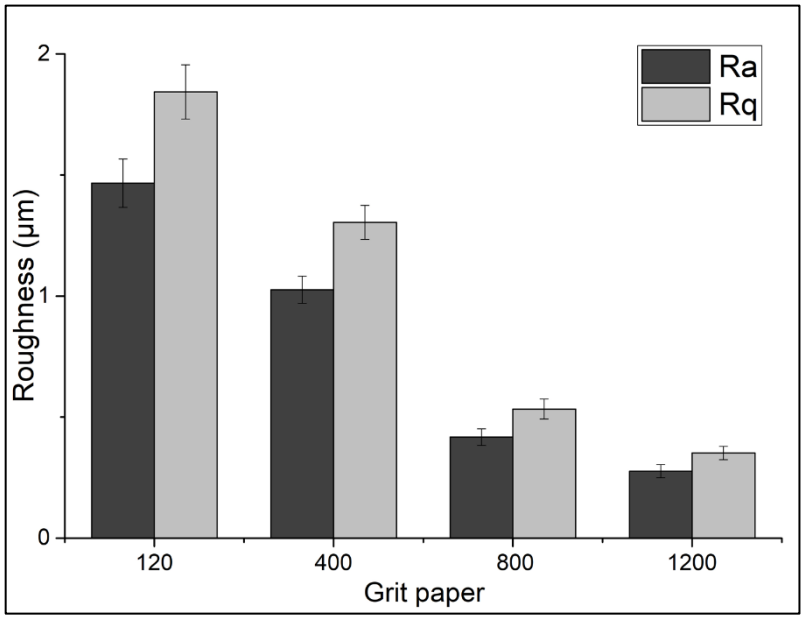

Figure 4. Roughness values of the magnesium substrates treated with different grit paper sizes.

3.2 Coating assessment

Figure 5 shows the coatings deposited on the substrates with the four different roughness values. In this case, the grinding lines were perpendicular (horizontal) to the withdrawal direction during the dip-coating process (Figure 2a). On the other hand, Figure 6 shows the coatings deposited on the substrates with the four different roughness values but, in this case, the grinding lines were parallel (vertical) to the withdrawal direction during the dip-coating process (Figure 2b).

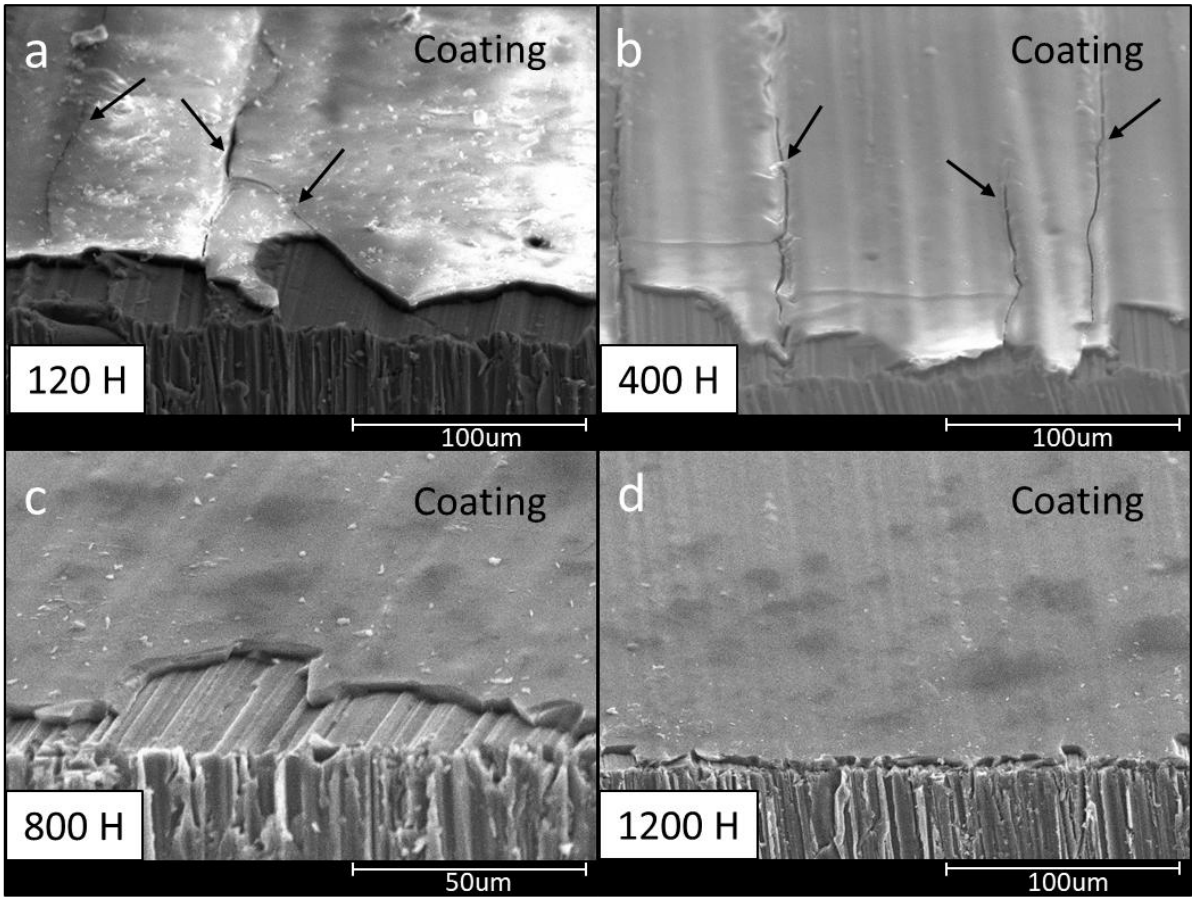

Figure 5. Sol-gel coatings deposited on Mg substrates with grinding lines perpendicular (horizontal) to the withdrawal direction during the dip-coating process. (a) Substrate grounded with 120 grit paper. (b) Substrate grounded with 400 grit paper. (c) Substrate grounded with 800 grit paper. (d) Substrate grounded with 1200 grit paper.

In both cases, horizontal and vertical grinding lines, the coatings on the substrates with the higher roughness values, obtained with 120 and 400 grit papers, appeared cracked and full of

defects. However, these defects presented different morphologies depending on the direction of the grinding lines. In the case of horizontal lines, continuous cracks were present along the grinding lines (arrows marked in Figures 5a and 5b). But in the case of vertical grinding lines, non-continuous defects were present instead of continuous cracks. These defects consisted of separated pores in the coating, distributed in queues following the direction of the grinding lines (arrowed zones in Figures 6a and 6b).

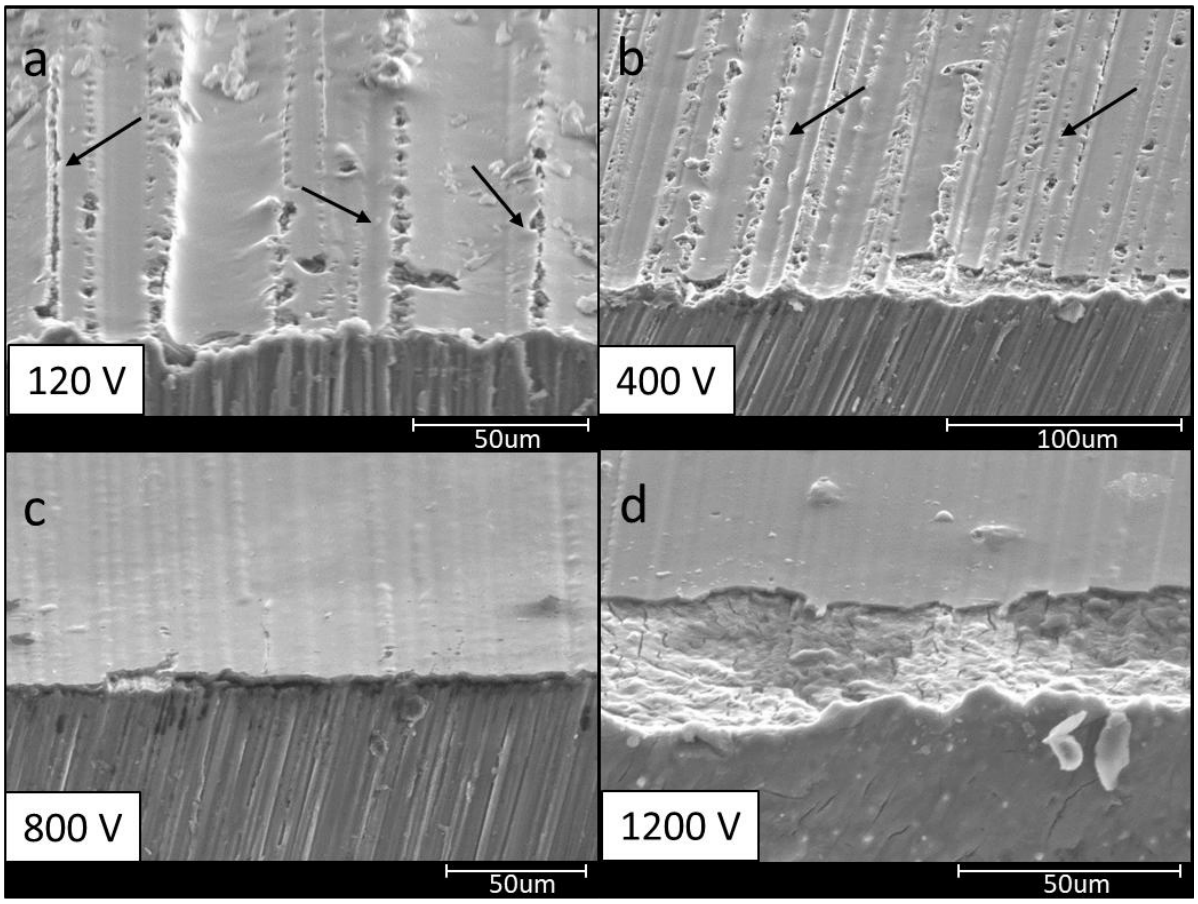

Figure 6. Sol-gel coatings deposited on Mg substrates with grinding lines parallel (vertical) to the withdrawal direction during the dip-coating process. (a) Substrate grounded with 120 grit paper. (b) Substrate grounded with 400 grit paper. (c) Substrate grounded with 800 grit paper. (d) Substrate grounded with 1200 grit paper.

For lower roughness values, no cracks or defects were visible in the coatings for horizontal (Figures 5c and 5d) nor vertical (Figures 6c and 6d) grinding lines.

The relation between the coating thickness, the roughness of the substrates, and the direction of the grinding lines for all the samples was studied by linear regression and analysis of

variance. Figure 7 depicts the plot of coating thickness values versus the roughness of the substrates for the two different grinding lines directions. Moreover, Table III shows the values of coating thickness and substrate roughness (*Ra*) for each sample, corresponding with the values of Figure 7.

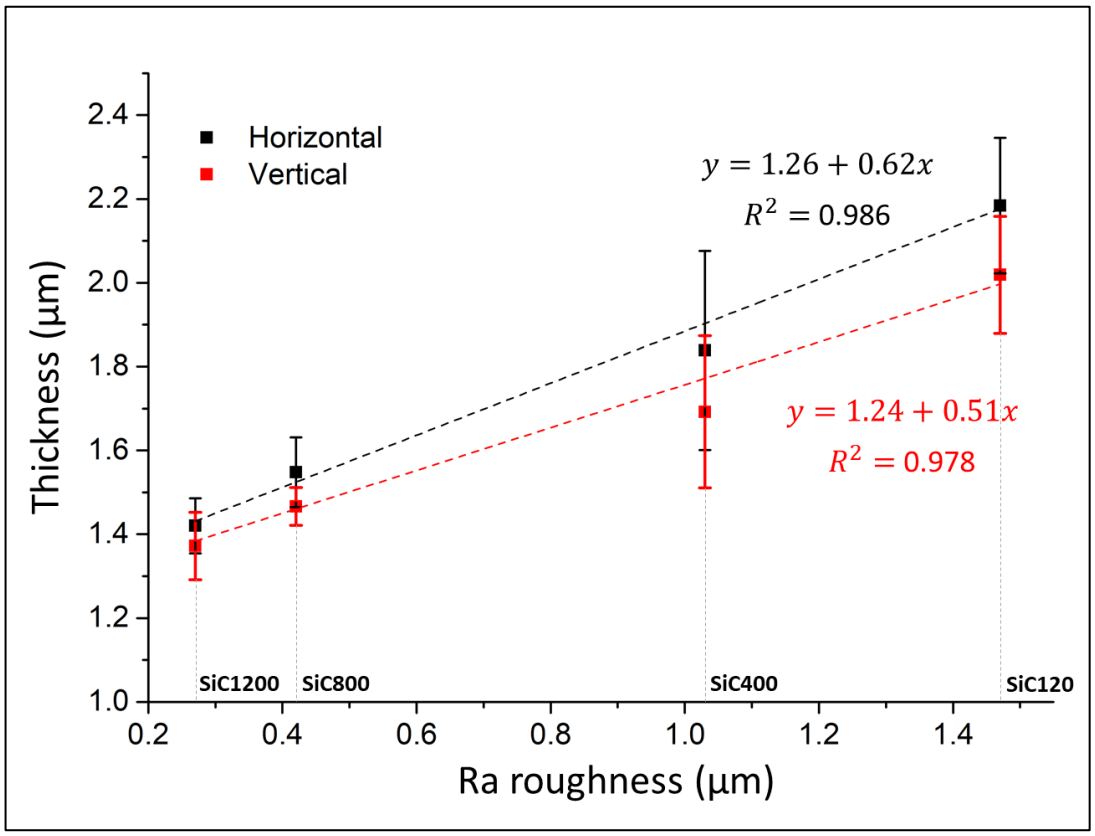

Figure 7. Relation between thickness and Ra roughness for the samples with horizontal and vertical grinding lines.

Table III. Roughness (Ra) and coating thickness average and standard deviation values.

Sample	*Ra* (µm)	Coating thickness (µm)
120 H	1.47 ± 0.09	2.18 ± 0.16
400 H	1.03 ± 0.05	1.83 ± 0.23
800 H	0.42 ± 0.03	1.54 ± 0.08
1200 H	0.27 ± 0.02	1.42 ± 0.06
120 V	1.47 ± 0.09	2.01 ± 0.13
400 V	1.03 ± 0.05	1.69 ± 0.18
800 V	0.42 ± 0.03	1.46 ± 0.04
1200 V	0.27 ± 0.02	1.37 ± 0.08

Through a linear regression of the values in Figure 7, it is possible to see that there is a correlation between the roughness of the coated samples and the final thickness of the

coatings deposited on them. Thus, the higher values of coating thickness are obtained for rougher surfaces. The values of the adjusted coefficient of determination (adj. R^2) and Pearson correlation coefficient (r) for the horizontal and vertical grinding lines models are shown in Table IV.

Table IV. Coefficients from linear regression.

Grinding direction	Adjusted R^2	Pearson's *r*
Horizontal	0.986	0.995
Vertical	0.978	0.992

It is also possible to see that there are no significant differences, in terms of coating thickness, between the samples with horizontal and vertical grinding lines, although mean coating thickness values are always slightly higher for the samples with horizontal grinding lines. Moreover, the higher the roughness of the substrate, the bigger the difference of mean coating thickness values between the samples with the two different grinding lines directions. Thus, in the case of the lowest roughness value (*Ra* = 0.27 µm) obtained with 1200 grit paper, the difference in coating thickness between the sample with the horizontal grinding lines (1.42 µm) and the sample with the vertical grinding lines (1.37 µm) is 0.05 µm (3.5 %). While in the case of the highest roughness value (*Ra* = 1.47 µm) obtained with 120 grit paper, the difference in coating thickness between the sample with the horizontal grinding lines (2.18 µm) and the sample with the vertical grinding lines (2.01 µm) is 0.17 µm (7.8 %).

3.3 Hydrophobicity

Figure 8 shows the contact angle for the samples with different grinding conditions. There were no significant differences between the contact angle values of the substrates treated with the 400, 800, and 1200 grit papers, which values were between 110º and 130º for all times. However, the mean values of the contact angle decreased when roughness values decreased.

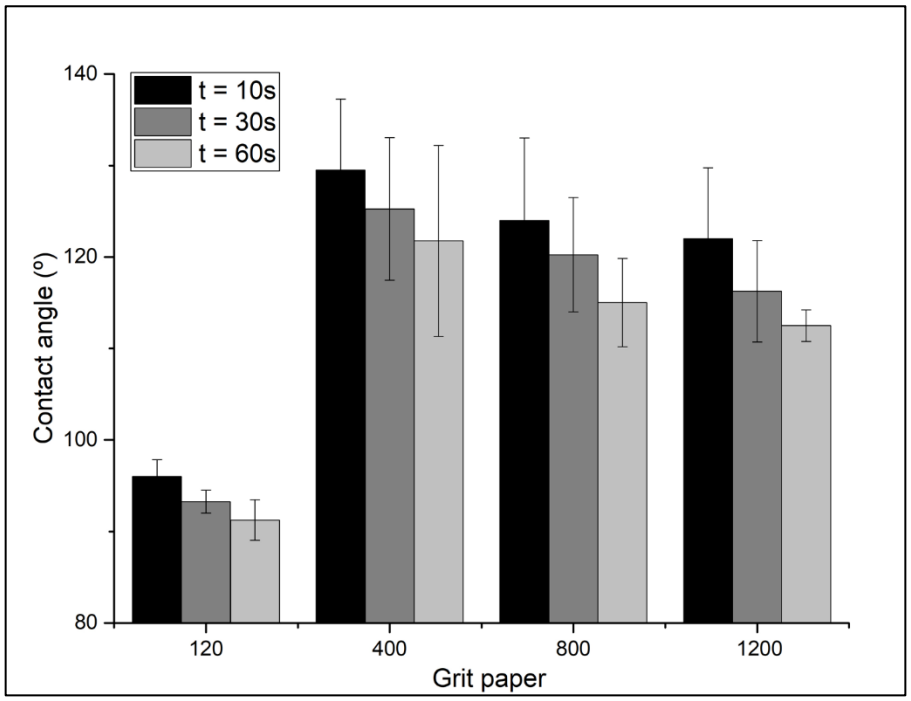

Figure 8. Contact angle for the magnesium substrates treated with the four different grit papers.

The contact angle for the substrate treated with the 120 grit paper, which presented the highest roughness values, was significantly smaller compared with the other cases, with values around 90 º, i.e., at the limit of wetting or not wetting the substrate.

3.4 Coating Adhesion tests

Figures 9 and 10 show the results of the adhesion tests for the samples with horizontal and vertical grinding lines. These graphs depict the maximum shear stress for all the coatings until the detachment or the cohesive failure of the coatings. The maximum loads, over 20 MPa, were obtained for the substrates with higher roughness values and thicker coatings, 120H and 400H in the case of substrates with horizontal grinding lines, and 120V and 400V in the case of substrates with vertical grinding lines. In the case of the 800H sample, the shear stress value was around 18.5 MPa, which is an intermediate value between the highest values, and the lowest ones, which corresponded to the 1200H, 800V, and 1200V, which were around 15 MPa. From these data, it is possible to determine that the direction of the grinding lines does not seem to play an important role in the adhesion of the coatings because no significant

differences were found. However, the roughness of the substrates influences the shear stress withstood by the coatings. In general, the higher the roughness, the higher the maximum shear stress resisted by the system.

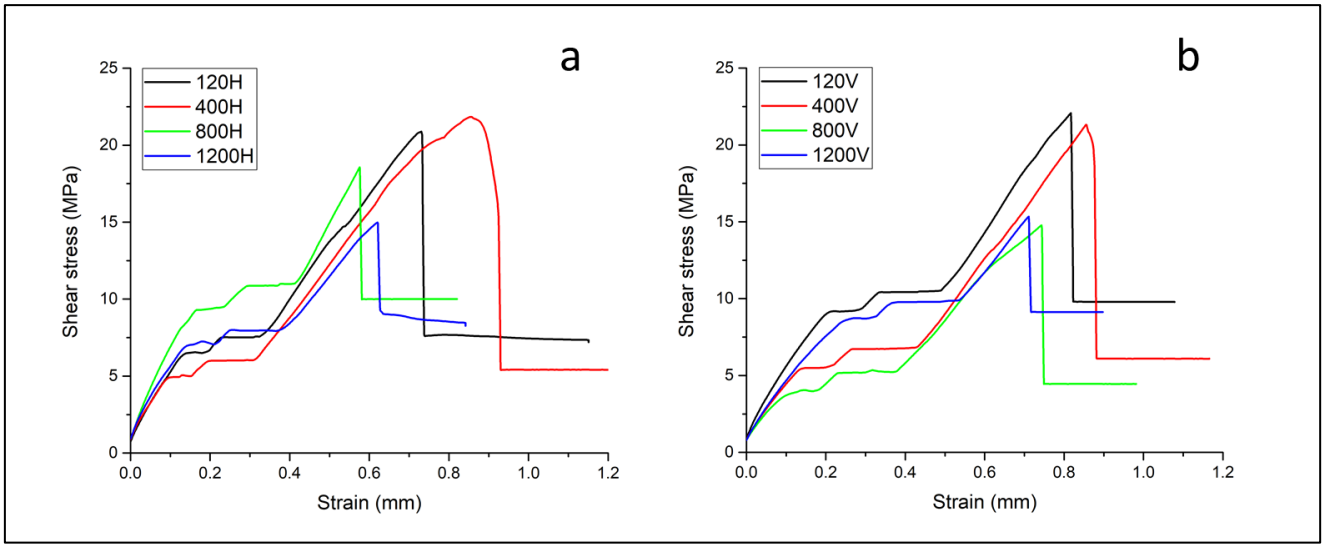

Figure 9. Shear stress of the coatings for the different horizontal grinding conditions (a) and vertical grinding conditions (b).

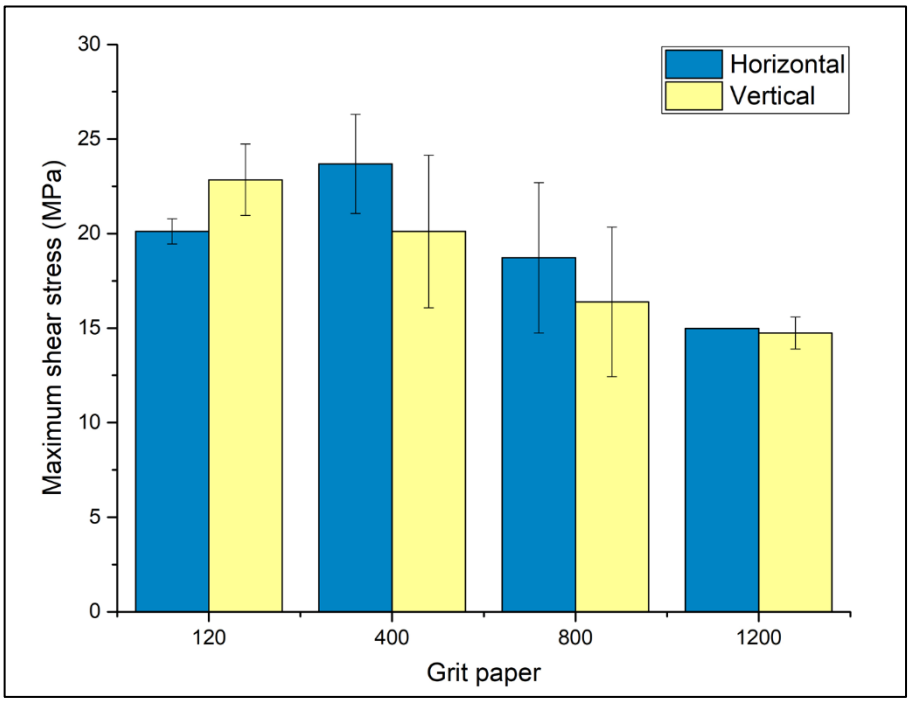

Figure 10. Maximum shear stress values for the tested samples with different grinding conditions.

Furthermore, the type of failure of the coating during the adhesion tests was influenced by the direction of the grinding lines, as it can be seen in Figures 11 and 12, which show the SEM micrographs of the surface of the different samples after the adhesion tests.

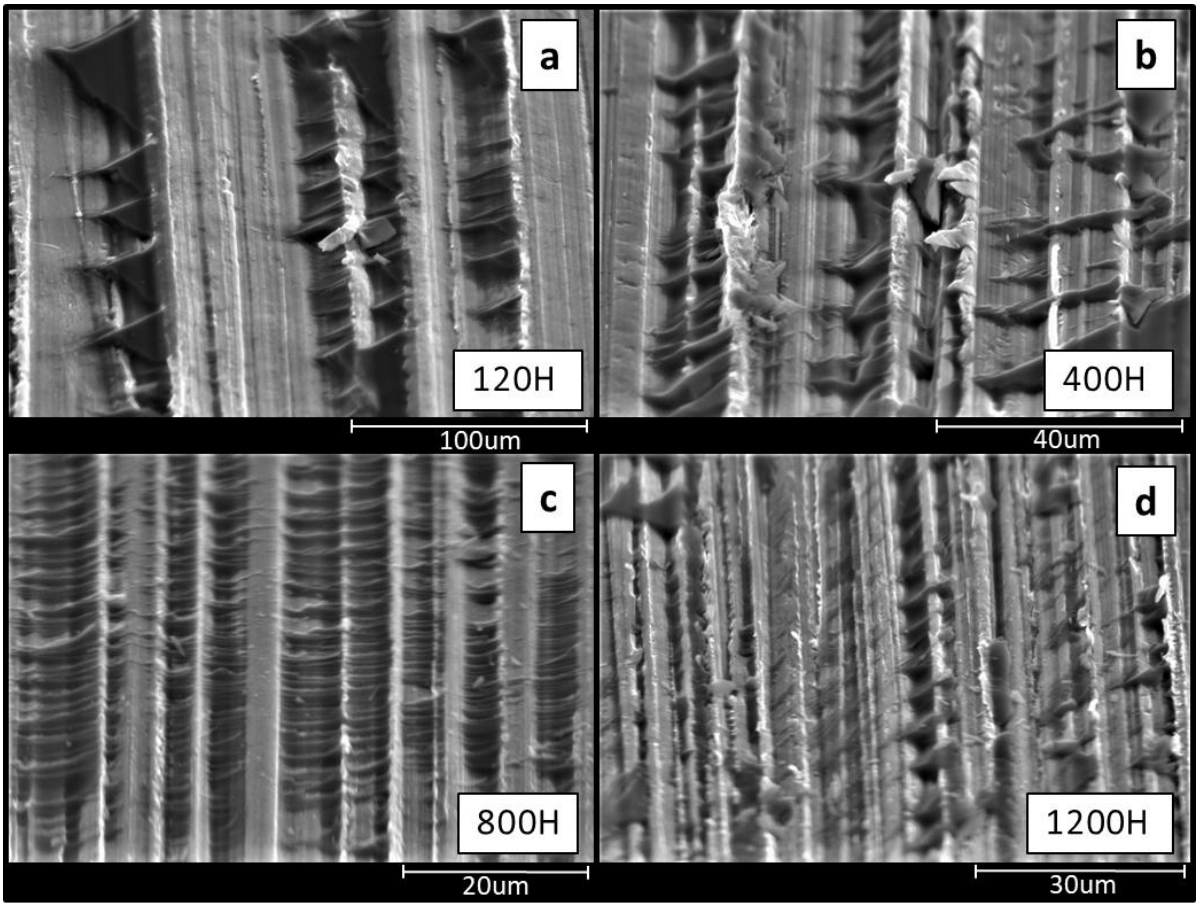

Figure 11. SEM micrographs of the surface of the substrates with different grinding conditions (a) 120H, (b) 400H, (c) 800H, and (d) 1200H after testing the adhesion of the coatings.

In the case of the samples with horizontal grinding lines (Figure 11), the rests of the coatings that remained on the surface of the substrate after the adhesion tests showed triangular and elongated morphologies, located inside the concave zones of the grooves. For the substrates with the highest roughness values, the grooves were deeper and, subsequently, larger amounts of coating remained on the substrates (Figures 11a and 11b). For lower values of roughness (Figures 11c and 11d), the remaining coating was also located inside the grooves but, in this case, smaller amounts of coating were found. The SEM micrographs indicate that cohesive

failure of the coating occurred inside the grooves, where high amount of coating accumulated. However, adhesive failure of the coating occurred outside the concave zones of the grooves, where almost no traces of coating were found.

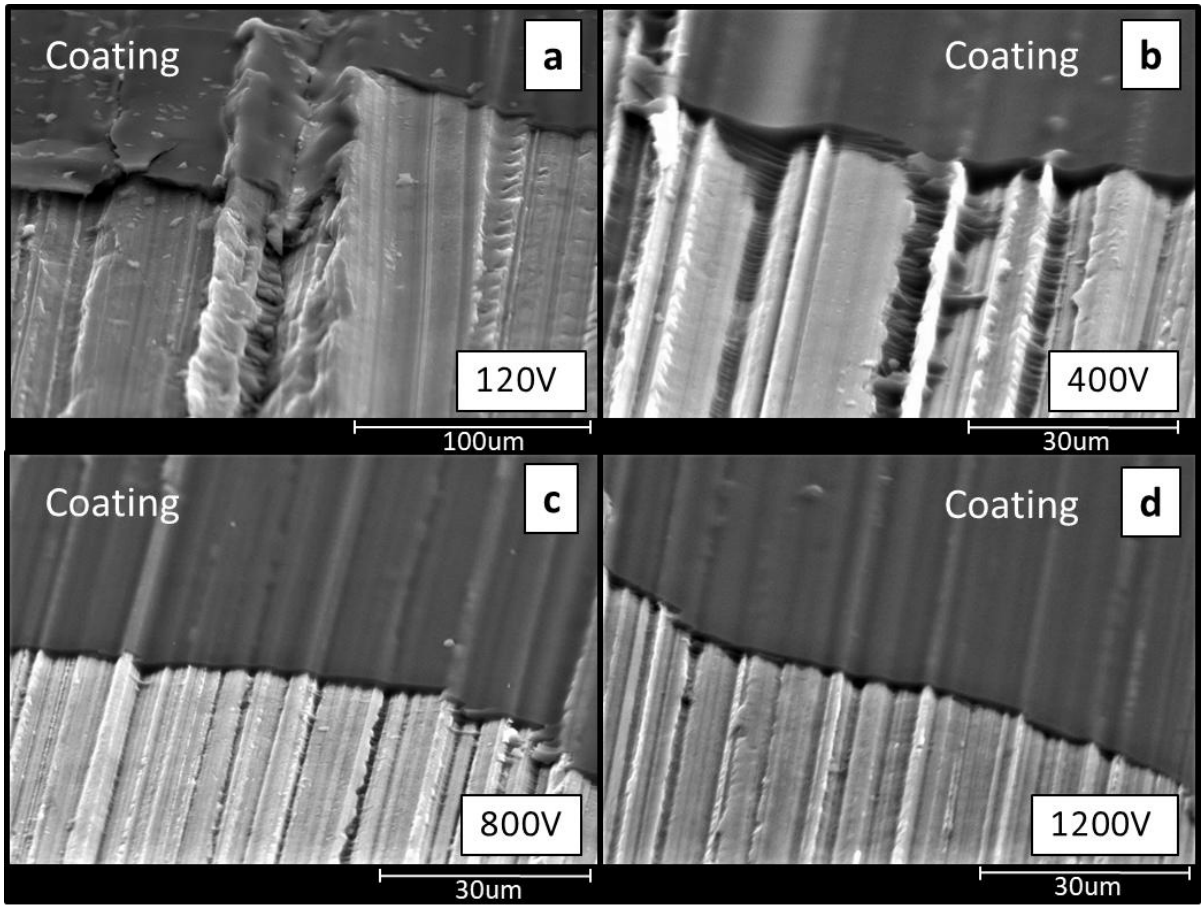

Figure 12. SEM micrographs of the surface of the substrates with different grinding conditions (a) 120V, (b) 400V, (c) 800V, and (d) 1200V after testing the adhesion of the coatings.

The SEM micrographs of the samples with vertical grinding lines (Figure 12) show that the remaining coating can be found only on the substrates with the highest roughness values, located inside the deepest grooves (Figures 12a and 12b), but in a lower amount compared with the substrates with horizontal grinding lines and only near to the edge of the test area. Outside the grooves, no traces of coating were found. For the substrates with lower roughness values, (Figures. 12c and 12d), no traces of coating were found inside nor outside the grooves over the tested area, which indicates an adhesive failure of the coatings.

4. Discussion

4.1 Coating assessment

When a material in a fluid state is deposited on the surface of a solid substrate to create a coating, the surface characteristics of the substrate play an important role in the final properties of the solid layer. Thus, roughness is an important factor that can modify the surface energy and, therefore, the hydrophobicity of the substrate, which can affect the amount of liquid remaining on the surface of the substrate and, consequently, the final thickness of the coating.

Hydrophobicity test showed that higher *Ra* values lead to higher mean contact angle values. This trend was fulfilled for the samples grounded with 400, 800, and 1200 grit papers, but without significant differences between these samples. However, this trend changed for the sample grounded with 120 grit paper. This sample presented the highest *Ra* value but the lowest contact angle value. Studies can be found in the literature that have determined that, in general, a higher substrate roughness value increases the hydrophobicity of the material [45, 47], but exceptions can occur for surfaces with high roughness values. Thus, this behaviour could be explained due to the existence of a limit roughness value from which the trend is inverted and the hydrophobicity starts to decrease as the roughness increase [48, 49].

In SEM images it is possible to observe that for roughness values higher than 1 μm (Figures 5a, 5b, 6a, and 6b), the coatings were damaged. Moreover, the morphologies of the defects in the coatings are different depending on the direction of the grinding lines on the surface of the substrate, horizontal or vertical regards to the dipping direction. In the case of horizontal lines, cracks were observed spreading along the direction of the grinding lines. In the case of vertical lines, separated pores aligned in the direction of the grinding lines were observed. The way that these defects are distributed indicates an anisotropy in the coatings, which decreases their mechanical properties in the direction of the grinding lines. That could be a consequence of the *Ra* values being 67 % of the value of coating thickness for 120H samples and 73 % of

the value of coating thickness for 120V samples, these high *Ra* values seem to affect the coating above the substrate, making it difficult for the sol-gel to totally cover the substrate at some points and increasing the presence of residual stress during the consolidation of the coating due to its reduction in thickness, affected by the heterogeneity of the substrate. Thus, non-compact, heterogeneous, or cracked coatings are obtained on the surface of these substrates.

The differences in the morphologies of the defects depend on the direction of the grinding lines with respect to the extraction direction during the dip-coating process. Thus, as it is shown in Figure 13, with horizontal lines oriented in the *X*-axis, perpendicular to the dip-coating extraction direction, oriented in the *Y*-axis, the sol-gel covered the whole surface because the grooves of the grinding lines help to drag more material during the extraction of the substrate from the sol-gel (Figure 13a). Before drying, part of the sol-gel falls downwards over the surface. Once the sol-gel is dried and the coating is created, in the case of high roughness values, although the surface is completely covered some cracks appear, especially in the coatings deposited on the surfaces with the higher roughness values (Figures 5a and 5b). This cracking event takes place because of the effect of residual stress during the consolidation of the coating due to its reduction in thickness, affected by the heterogeneity of the substrate. These cracks grow following the direction of the grinding lines, originated at the points of lower thickness, marked with arrows in Figure 13b.

On the other hand, as it is shown in Figure 14, in the case of vertical lines oriented in the *Y*-axis, parallel to the dip-coating extraction direction, also oriented in the *Y*-axis, the amount of material dragged from the sol-gel during the extraction of the substrate is lower than in the previous case (Figure 14a). While the sample is being pulled, the sol-gel runs off the surface. In this case, as the direction of the extraction matches with the direction of the grinding lines, the sol-gel is not forced to coat the peaks in the surface and tends to accumulate in the concave areas of the grooves. Consequently, there is a lack of coating material in some points

of the ridges of the grooves, (arrowed zones in Figure 14b), creating these aligned hollow defects shown in Figures. 6a and 6b.

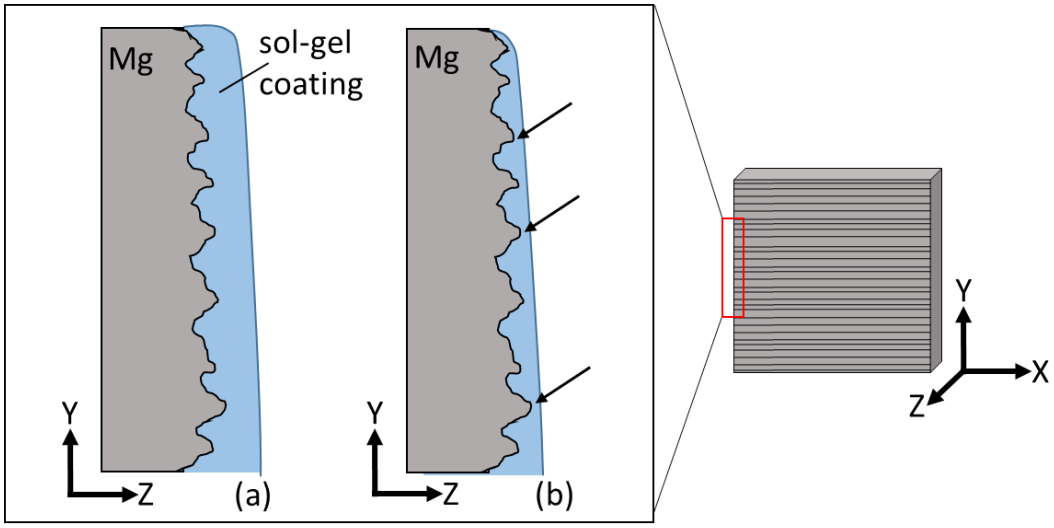

Figure 13. Coating mode in substrates with grinding lines in the horizontal direction. (a) Coating after dip-coating. (b) Coating after drying and sintering.

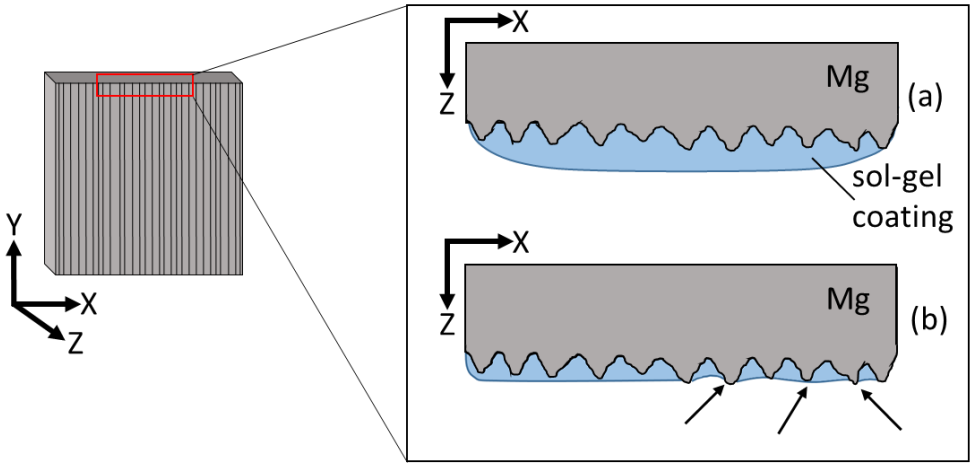

Figure 14. Coating mode in substrates with grinding lines in the vertical direction. (a) Coating after dip-coating. (b) Coating after drying and sintering.

For the samples with lower roughness values (Figures. 5c, 5d, 6c, and 6d), the dragged material from the sol-gel was enough to completely cover the surface of the substrates, regardless of the direction of the grinding lines. In the case of the 1200H and 1200V samples, the *Ra* value of the surface of these substrates (0.27 µm) represents 19 % of the thickness value for the coating on the 1200H sample (1.47 µm), and 20 % of the thickness value for the coating on the 1200V sample (1.37 µm). Contrary to what happens for higher roughness

values, these *Ra* values are low enough to obtain homogeneous and defect-free coatings on the surface of these substrates. However, the thickness of the coatings of the substrates with horizontal grinding lines is always higher compared with the coatings of the substrates with vertical grinding lines, because in the first case, the drag of material from the sol-gel is always higher (Figure 7), which means that these coatings would be more interesting for practical applications.

The direct correlation between substrate roughness and final coating thickness was demonstrated through the linear regression of the data in Figure 7, and the values of the adjusted coefficient of determination (adj. R^2) and Pearson correlation coefficient (r) from Table IV. The values of adjusted R^2 and Pearson's r are very close to 1 for both linear regressions, which indicates that the linear models fit the data and there is a strong positive correlation between substrate roughness and coating thickness.

4.2 Analysis of variance

To study the dependence of the coating thickness on the two different factors studied in this research, roughness and grinding lines direction, an analysis of variance was carried out. Figure 15 shows the coating thickness values for each factor compared with the average thickness value for all the samples, represented by the horizontal dotted line. The data obtained from the analysis of variance are shown in Table V.

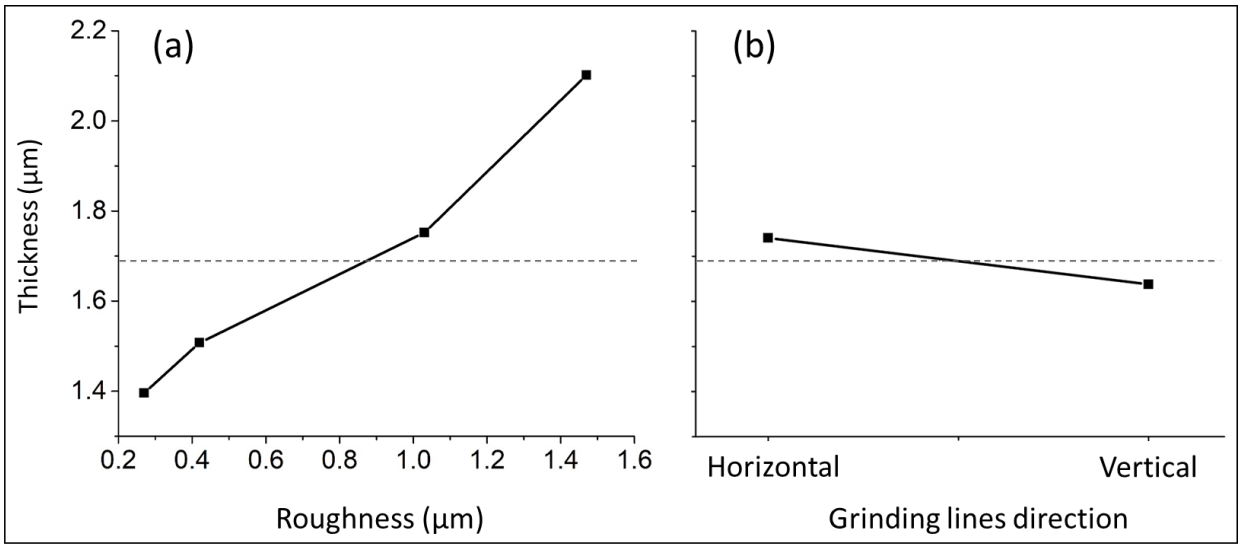

Figure 15 Dependence of the coating thickness on the roughness of the substrate (a) and the direction of the grinding lines (b).

Table V. Results obtained from the analysis of variance related to coating thickness.

Factors	Thickness (µm)				
	SS	DF	F	p	% of contribution
Roughness	7.60	3	117.10	$5.8 \cdot 10^{-32}$	78.54 %
Grinding direction	0.26	1	2.75	0.101	2.73 %

From the study of the dependence of coating thickness on the different factors, Figure 15a indicates that the thickness values are higher for higher roughness values and there is dependence on this factor. However, in Figure 15b the thickness values for both grinding directions are very close to the average value, which indicates that there is almost no dependence on this factor.

The results obtained in the analysis of variance (Table V) for the roughness factor indicate that the null hypothesis can be rejected ($p = 5.8 \cdot 10^{-32} < 0.05$). Therefore, the roughness is a significant factor in the coating thickness value and its contribution to the coating thickness is 78.54 %. However, for the grinding direction factor, the null hypothesis cannot be rejected since $p = 0.101 > 0.05$, which means that this is not a significant factor in the coating thickness value. Moreover, its contribution to the coating thickness is only 2.73 %.

4.3 Coating adhesion

With regard to the adhesion of the coatings on the substrates with different grinding conditions, the differences between the samples with horizontal and vertical grinding lines can be explained through the evaluation of the surface of the samples after the shear stress tests. The assessment of the SEM micrographs of the surface of the samples, combined with the data extracted from the shear stress tests, show that the roughness of the substrates mainly influences the shear stress withstood by the coating, and the direction of the grinding lines mainly influences how the coatings fail during the tests.

The highest shear stress values were obtained for the coatings deposited on the substrates with the highest roughness values, 120H and 400H in the case of substrates with horizontal grinding lines, and 120V and 400V for the substrates with vertical grinding lines. On these substrates, rests of the coatings were found inside the concave areas of the grooves, especially on the substrates with horizontal grinding lines (Figures 11a, 11b, 12a, and 12b), which indicates that the anchorage of the coatings to the substrates was better in these zones than in the flat zones or in the ridges of the grooves. Therefore, the higher shear stress values obtained for these samples were a consequence of the presence of deeper grooves on the surface of these substrates. Thus, higher shear stress values were obtained on substrates with higher surface roughness, regardless of the direction of the grinding lines.

However, the direction of the grinding lines influences the way that the coatings fail under shear stress, and the type of failure seems to be independent of the roughness of the substrate. For both grinding directions, horizontal and vertical, the adhesive failure of the coating is predominant, since the vast majority of the surface of the substrate is exposed after the shear stress tests. However, rests of the coatings can also be observed. For all the substrates with the horizontal grinding lines, these rests were dispersed over the tested area, aligned with the grinding lines, and extended in the direction of the applied shear stress (Figure 16a), but for the substrates with the vertical grinding lines, the amount of coating remaining on the surface was much lower and it was concentrated inside the biggest grooves, near the edge between the tested area and the non-tested coating (Figure 16b).

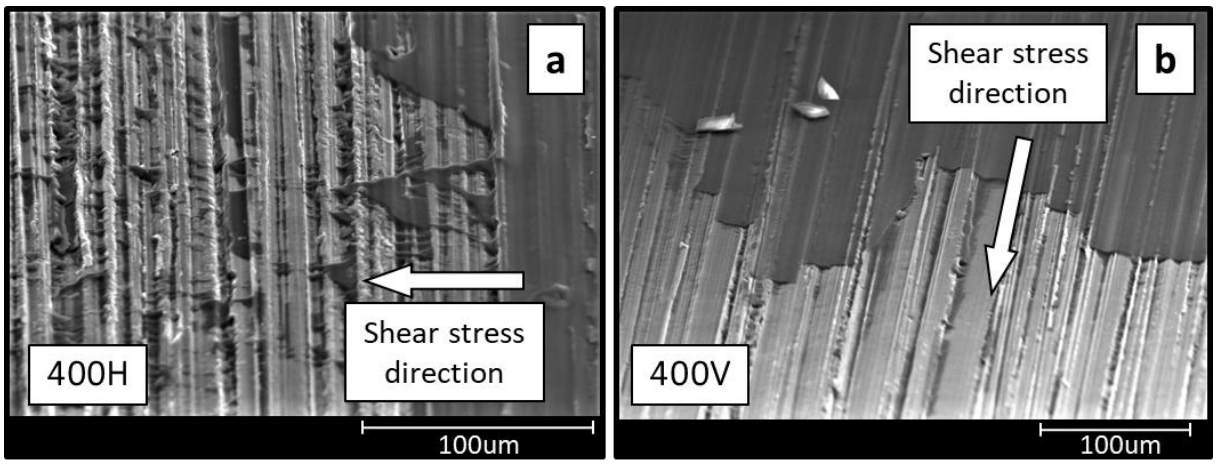

Figure 16. Surface of the substrates after shear stress tests. (a) Substrate with horizontal grinding lines. (b) Substrate with vertical grinding lines.

4.4 Calculation and validation of the proposed *r* parameter

Since the roughness of the substrate plays an important role in the final thickness of the coating deposited, a new parameter (*r*) is proposed to be included in the Landau-Levich equation to adjust it, considering the roughness of the substrate in the final thickness of the coating, which has been neglected until now. The proposed equation contains the *r* parameter, as it is shown in equation 2.

$$h = 0.94 \frac{(\eta \,.\, v)^{2/3}}{{\gamma_{LV}}^{1/6} (\rho \,.\, g)^{1/2}} \, r \tag{2}$$

Equation 3 can be obtained from equation 2. This equation can be used to calculate the values of the r parameter for the different tested samples.

$$r = \frac{h}{0.94 \frac{(\eta \,.\, v)^{2/3}}{{\gamma_{LV}}^{1/6} (\rho \,.\, g)^{1/2}}} \tag{3}$$

The values of the different parameters used in equation 3 are shown in Table VI.

Table VI. Parameters used in the calculation of *r*.

η (kg/(m.s)	v (m/s)	γ_{LV} (kg/(m.s^2)	ρ (kg/m^3)
0.0268	0.00583	2892.2	890

In equation 3, the r parameter depends on the average final thickness of the coating (*h*), and as it can be extracted from the analysis of variance, the thickness of the coating depends on the average roughness value of the substrate (*Ra*). Therefore a relation can be established between the r parameter and the average roughness of the substrate which is intended to be coated.

Since the direction of the grinding lines does not significantly affect the coating thickness, the experimental mean thickness value (*h*) used in equation 3 to calculate the *r* factor was obtained from the measured thickness values of the samples with both horizontal and vertical grinding lines for each roughness value. Table VII shows the calculated *r* parameter for each sample.

Table VII. Calculated r parameters for each coated sample from mean roughness (*Ra*) and mean coating thickness (*h*).

Sample	*Ra (µm)*	*h (µm)*	*r*
120 grit	1.47	2.1	0.271
400 grit	1.03	1.75	0.226
800 grit	0.42	1.51	0.195
1200 grit	0.27	1.4	0.181

The relation between the average substrate roughness (*Ra*) and the *r* parameter calculated from the mean coating thickness values (*h*), can be established using the values of Table VII, as it is shown in Figure 17.

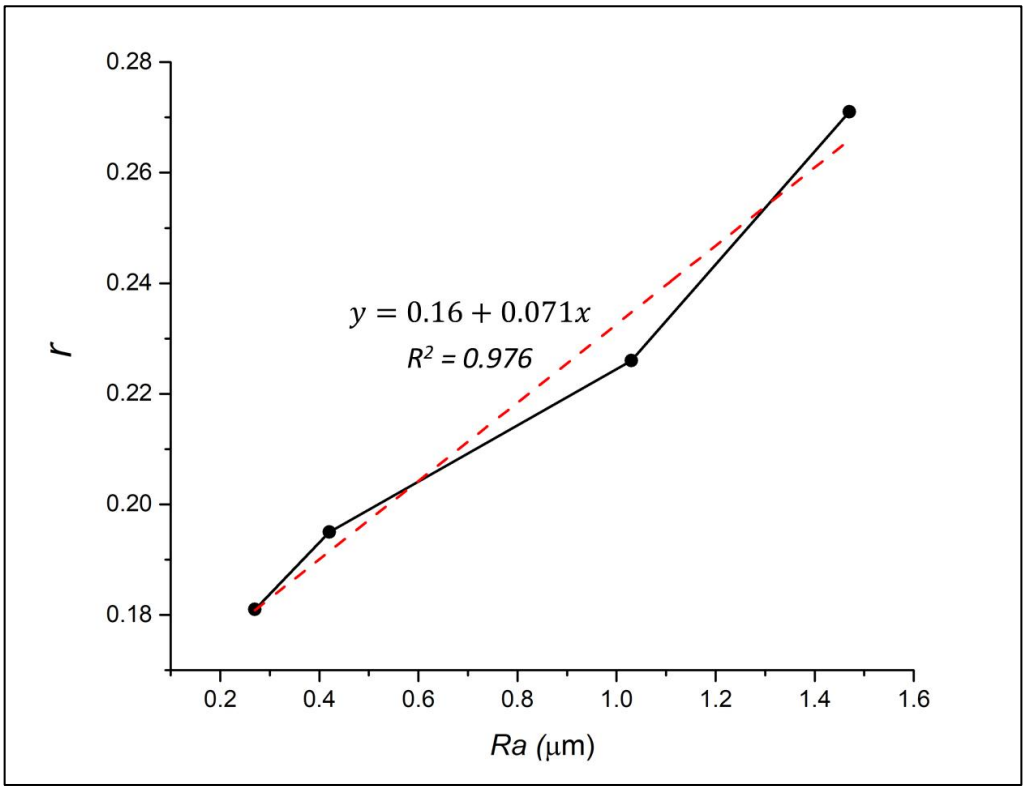

Figure 17. *r* parameters calculated for each *Ra* value from the substrates with the different grinding conditions.

The value of the *r* parameter depends on the average roughness value of the substrate (*Ra*). Equation 4, extracted from Figure 17, shows this dependence:

$$r = f(Ra) = 0.16 + 0.071Ra \quad (4)$$

Once the relation between *r* and *Ra* was determined, Table VIII and Figure 18 show the comparison between the average thickness values measured in the tested samples and the thickness values calculated with the proposed adjusted Landau-Levich equation (equation 2).

Table VIII. Comparison of the values of the measured and calculated *h*, in relation to the different roughness values.

Sample	*Ra (μm)*	*Measured h (μm)*	*Calculated h (μm)*
120 grit	1.47 ± 0.09	2.1 ± 0.17	2.05
400 grit	1.03 ± 0.05	1.75 ± 0.22	1.81
800 grit	0.42 ± 0.03	1.51 ± 0.08	1.48
1200 grit	0.27 ± 0.02	1.4 ± 0.08	1.39

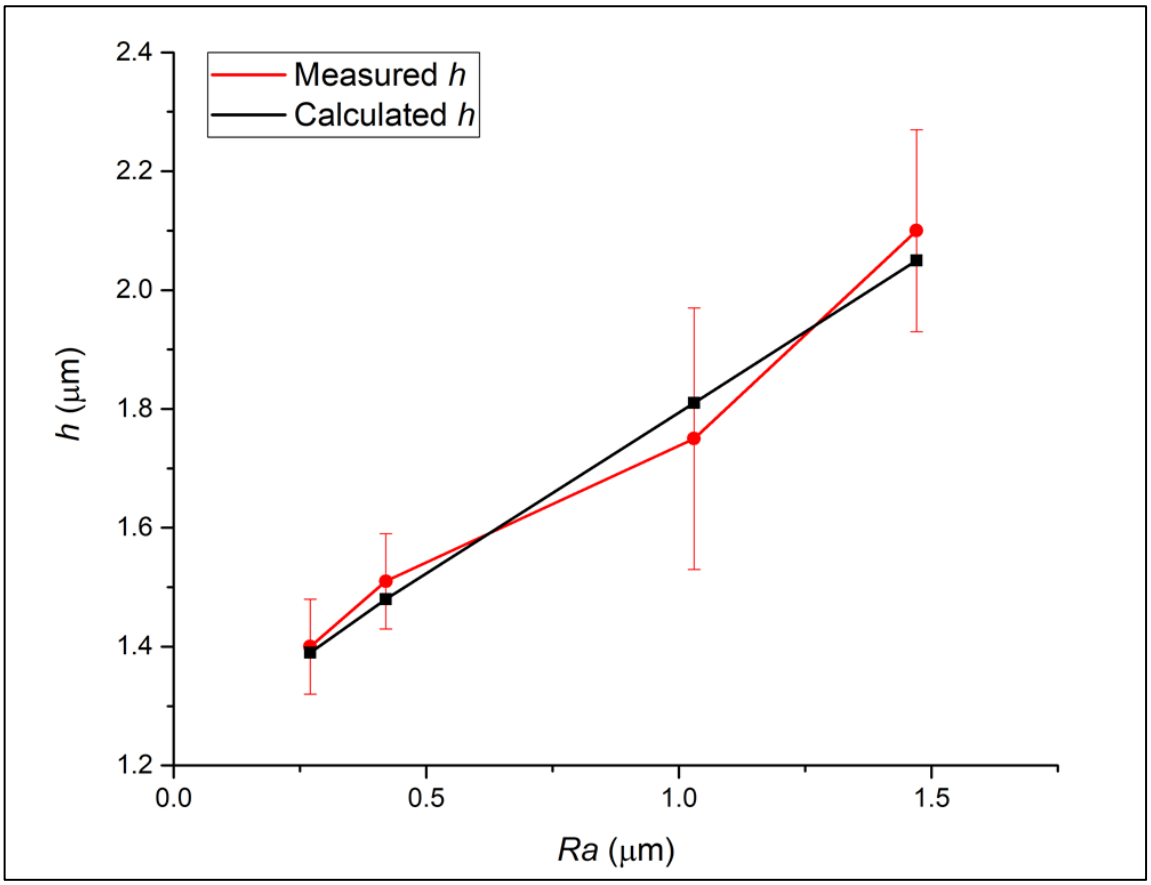

Figure 18. Comparison between the coating thicknesses (h) measured on the samples and the thickness values calculated with the proposed adjusted Landau-Levich equation considering the roughness (*Ra*) values of the substrates.

In the case where $Ra = 0$, the r parameter takes the value $r = 0.16$, as it can be extrapolated from equation 4. In this case, using this value of the r parameter in equation 2, the value of the thickness (h) calculated with the adjusted Landau-Levich equation takes the value $h = 1.23$ µm. However, if the thickness of the coating is calculated using the original Landau-Levich equation (equation 1), in which the effect of the roughness is neglected, and therefore no r parameter is considered, the thickness takes the value $h = 7.7$ µm. Contrary to the values obtained, it would be expected that both values of h were close to each other because no roughness was considered in any case. However, this inconsistency could be explained because the r parameter used in the adjusted Landau-Levich equation (equation 2) considers not only the effect of the roughness but the effect of the evaporation of liquid phases during the dip-coating, as outlined below.

Equation 1 can be used to calculate the thickness at the point where the viscous drag, the gravity force, and the liquid-vapour surface tension are balanced during the extraction of the substrate from the sol-gel during the dip-coating [22]. This thickness corresponds with $h_{L\text{-}L}$ in Figure 19. However, during the extraction of the substrate from the sol-gel, some of the solvent and water evaporate with the consequent reduction in the thickness of the coating until the value h_o, showed in Figure 19. However, in the coating with thickness value h_o some liquid phases are still present.

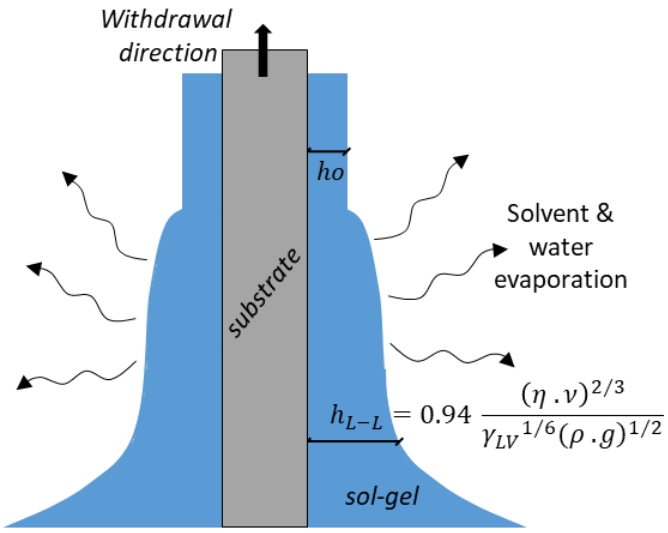

Figure 19. Scheme of the profile of the liquid dragged on the surface of a moving plate during the dip-coating method, adapted from C.J. Brinker et al. [22].

Therefore, the coated samples were subjected to a drying and sintering heat treatment to eliminate the liquid phases still present in the coating, obtaining the coating with the final thickness (h), which value is much thinner than the thickness calculated using the Landau-Levich equation ($h_{L\text{-}L}$) (equation 1). The thickness (h) was the mean thickness value measured by scanning electron microscopy and used in equation 3 to calculate the r parameter for each grinding condition. Therefore, the inconsistency is explained because the original Landau-Levich equation neglects not only the effect of roughness but the evaporation of the liquid phases. However, the r parameter was calculated considering both the effect of roughness and that of the evaporation of the liquid phases.

A test was carried out to determine the loss of volume of the sol-gel during the drying and sintering heat treatment. In these tests, 30 mL of sol-gel in liquid state were subjected to the heat treatment used on the coated samples. At the end of the test, a final volume of 3.4 mL was measured for the remaining solid. Therefore, the volume was reduced by 88.6 %. This value can be used to calculate the final thickness using the Landau-Levich equation (equation 1), but this time including the effect of the evaporation of the liquid phases. Thus, the final thickness after the heat treatment was 11.3 % of the initial thickness, which value was 7.7 µm. Thus, the thickness value calculated using equation 1, after the heat treatment, was 0.87 µm. Much thinner than the initial thickness and closer to the value calculated using the adjusted Landau-Levich equation (equation 2), which value was 1.23 µm.

The thickness values calculated using the Landau-Levich equation adjusted with the r parameter were very close to the real values, which were measured directly on the samples. Thus, we propose the use of the *r* parameter as a first approximation to obtain more accurate thickness values which, through the use of this parameter, are calculated taking into account the evaporation of liquid phases from the sol-gel coating, and the roughness of the surface of the substrate, which was demonstrated to play an important role in the final thickness of the coatings.

5. Conclusions

The roughness of the substrate plays an important role in the thickness of the sol-gel coatings deposited on their surfaces. Therefore, roughness must be considered when performing a dip-coating process from a sol-gel. However, the direction of the grinding lines was not a significant factor affecting the coating thickness, but it had a clear influence on the morphology of the defects present in some coatings. The adhesion strength of the coatings was higher on the substrates with higher roughness values due to the presence of bigger grooves, where a better anchorage of the coatings was found. The best coatings, in terms of thickness and absence of defects, were obtained on samples grounded with 1200 and 800 grit

papers, with thickness values around 1.4 µm. Finally, a new *r* parameter was proposed in the Landau-Levich equation, that considers the roughness of the substrates intended to be coated, and the reduction of the thickness of the sol-gel coatings due to the evaporation of the liquid phases during the dip-coating, that can help to calculate more accurately the thickness of the coatings.

6. Acknowledgment

The authors would like to acknowledge Ministerio de Ciencia e Innovación (FPI grant BES-2016-076946), Agencia Estatal de Investigación (RTI 2018-0963-B-C31) and Comunidad de Madrid Project ADITIMAT-CM (S2018/NMT-4411) for their economic support.

References

[1] N. Li, Y. Zheng, Novel Magnesium Alloys Developed for Biomedical Application: A Review, J. Mater. Sci. Technol. 29 (2013) 489–502. https://doi.org/10.1016/j.jmst.2013.02.005.

[2] M. Niinomi, M. Nakai, J. Hieda, Development of new metallic alloys for biomedical applications, Acta Biomater. 8 (2012) 3888–3903. https://doi.org/10.1016/j.actbio.2012.06.037.

[3] M.P. Staiger, A.M. Pietak, J. Huadmai, G. Dias, Magnesium and its alloys as orthopedic biomaterials: A review, Biomaterials. 27 (2006) 1728–1734. https://doi.org/10.1016/j.biomaterials.2005.10.003.

[4] X.N. Gu, S.S. Li, X.M. Li, Y.B. Fan, Magnesium based degradable biomaterials: A review, Front. Mater. Sci. 8 (2014) 200–218. https://doi.org/10.1007/s11706-014-0253-9.

[5] M.K. Kulekci, Magnesium and its alloys applications in automotive industry, Int. J. Adv. Manuf. Technol. 39 (2008) 851–865. https://doi.org/10.1007/s00170-007-1279-2.

[6] T. Kaneko, M. Suzuki, Automotive applications of magnesium alloys, Mater. Sci. Forum. 419–422 (2003) 67–72. https://doi.org/10.4028/www.scientific.net/msf.419-422.67.
[7] H. Friedrich, S. Schumann, Research for a “new age of magnesium” in the automotive industry, J. Mater. Process. Technol. 117 (2001) 276–281. https://doi.org/10.1016/S0924-0136(01)00780-4.
[8] S. Yoshizawa, A. Brown, A. Barchowsky, C. Sfeir, Role of magnesium ions on osteogenic response in bone marrow stromal cells, Connect. Tissue Res. 55 (2014) 155–159. https://doi.org/10.3109/03008207.2014.923877.
[9] S. Yoshizawa, A. Brown, A. Barchowsky, C. Sfeir, Magnesium ion stimulation of bone marrow stromal cells enhances osteogenic activity, simulating the effect of magnesium alloy degradation, Acta Biomater. 10 (2014) 2834–2842. https://doi.org/10.1016/j.actbio.2014.02.002.
[10] R.W. Li, N.T. Kirkland, J. Truong, J. Wang, P.N. Smith, N. Birbilis, D.R. Nisbet, The influence of biodegradable magnesium alloys on the osteogenic differentiation of human mesenchymal stem cells, J. Biomed. Mater. Res. - Part A. 102 (2014) 4346–4357. https://doi.org/10.1002/jbm.a.35111.
[11] J.P. Fernández-Hernán, A.J. López, B. Torres, J. Rams, Silicon oxide multilayer coatings doped with carbon nanotubes and graphene nanoplatelets for corrosion protection of AZ31B magnesium alloy, Prog. Org. Coatings. 148 (2020) 105836. https://doi.org/10.1016/j.porgcoat.2020.105836.
[12] A.J. López, J. Rams, A. Ureña, Sol-gel coatings of low sintering temperature for corrosion protection of ZE41 magnesium alloy, Surf. Coatings Technol. 205 (2011) 4183–4191. https://doi.org/10.1016/j.surfcoat.2011.03.011.
[13] K. Chen, J. Dai, X. Zhang, Improvement of corrosion resistance of magnesium alloys for biomedical applications, Corros. Rev. 33 (2015) 101–117. https://doi.org/10.1515/corrrev-2015-0007.
[14] J. Yang, F. Cui, I.S. Lee, Surface modifications of magnesium alloys for biomedical applications, Ann. Biomed. Eng. 39 (2011) 1857–1871. https://doi.org/10.1007/s10439-011-0300-y.
[15] Q. Li, Sol-gel coatings to improve the corrosion resistance of magnesium (Mg) alloys, Corros. Prev. Magnes. Alloy. A Vol. Woodhead Publ. Ser. Met. Surf. Eng. (2013) 469–485. https://doi.org/10.1533/9780857098962.3.469.
[16] R.B. Figueira, C.J.R. Silva, E. V. Pereira, Organic–inorganic hybrid sol–gel coatings for metal corrosion protection: a review of recent progress, J. Coatings Technol. Res. 12 (2014) 1–35. https://doi.org/10.1007/s11998-014-9595-6.
[17] J.A. Picas, A. Forn, G. Matthäus, HVOF coatings as an alternative to hard chrome for pistons and valves, Wear. 261 (2006) 477–484. https://doi.org/10.1016/j.wear.2005.12.005.
[18] E.S. Bogya, Z. Károly, R. Barabás, Atmospheric plasma sprayed silica-hydroxyapatite coatings on magnesium alloy substrates, Ceram. Int. 41 (2015) 6005–6012. https://doi.org/10.1016/j.ceramint.2015.01.041.
[19] J. Charlesbabu, K. Gopalakrishnan, M. Elango, K. Vasudevan, Preparation and characterization of ZnO thin films by spin coating method, Inorg. Nano-Metal Chem. 47 (2017) 1298–1303. https://doi.org/10.1080/24701556.2016.1242627.
[20] D.B. Hall, P. Underhill, J.M. Torkelson, Spin coating of thin and ultrathin polymer films, Polym. Eng. Sci. 38 (1998) 2039–2045. https://doi.org/10.1002/pen.10373.
[21] L.E. Scriven, Physics and Applications of DIP Coating and Spin Coating, MRS Proc. 121 (1988) 717–729. https://doi.org/10.1557/proc-121-717.
[22] C.J. Brinker, G.C. Frye, A.J. Hurd, C.S. Ashley, Fundamentals of sol-gel dip coating, Thin Solid Films. 201 (1991) 97–108. https://doi.org/10.1016/0040-6090(91)90158-T.
[23] Y.J. Tarzanagh, D. Seifzadeh, Z. Rajabalizadeh, A. Habibi-Yangjeh, A. Khodayari, S.

Sohrabnezhad, Sol-gel/MOF nanocomposite for effective protection of 2024 aluminum alloy against corrosion, Surf. Coatings Technol. 380 (2019) 125038. https://doi.org/10.1016/j.surfcoat.2019.125038.
[24] S.A. Omar, J. Ballarre, Y. Castro, E. Martinez Campos, W. Schreiner, A. Durán, S.M. Cere, 58S and 68S sol-gel glass-like bioactive coatings for enhancing the implant performance of AZ91D magnesium alloy, Surf. Coatings Technol. 400 (2020) 126224. https://doi.org/10.1016/j.surfcoat.2020.126224.
[25] S. Nezamdoust, D. Seifzadeh, Z. Rajabalizadeh, Application of novel sol–gel composites on magnesium alloy, J. Magnes. Alloy. 7 (2019) 419–432. https://doi.org/10.1016/j.jma.2019.03.004.
[26] R. Samadianfard, D. Seifzadeh, A. Habibi-Yangjeh, Y. Jafari-Tarzanagh, Oxidized fullerene/sol-gel nanocomposite for corrosion protection of AM60B magnesium alloy, Surf. Coatings Technol. 385 (2020) 125400. https://doi.org/10.1016/j.surfcoat.2020.125400.
[27] C.A. Hernández-Barrios, C.A. Cuao, M.A. Jaimes, A.E. Coy, F. Viejo, Effect of the catalyst concentration, the immersion time and the aging time on the morphology, composition and corrosion performance of TEOS-GPTMS sol-gel coatings deposited on the AZ31 magnesium alloy, Surf. Coatings Technol. 325 (2017) 257–269. https://doi.org/10.1016/j.surfcoat.2017.06.047.
[28] S. Nezamdoust, D. Seifzadeh, Z. Rajabalizadeh, PTMS/OH-MWCNT sol-gel nanocomposite for corrosion protection of magnesium alloy, Surf. Coatings Technol. 335 (2018) 228–240. https://doi.org/10.1016/j.surfcoat.2017.12.044.
[29] P.C. Innocenzi, M. Guglielmi, M. Gobbin, P. Colombo, Coating of metals by the sol-gel dip-coating method, J. Eur. Ceram. Soc. 10 (1992) 431–436. https://doi.org/10.1016/0955-2219(92)90018-9.
[30] J.D. Mackenzie, Applications of the sol-gel process, J. Non. Cryst. Solids. 100 (1988) 162–168. https://doi.org/10.1016/0022-3093(88)90013-0.
[31] M. Atik, P. de Lima Neto, L.A. Avaca, M.A. Aegerter, Sol-gel thin films for corrosion protection, Ceram. Int. 21 (1995) 403–406. https://doi.org/10.1016/0272-8842(95)94466-N.
[32] L.L. Hench, J.K. West, The Sol-Gel Process, Chem. Rev. 90 (1990) 33–72. https://doi.org/10.1021/cr00099a003.
[33] D. Wang, G.P. Bierwagen, Sol-gel coatings on metals for corrosion protection, Prog. Org. Coatings. 64 (2009) 327–338. https://doi.org/10.1016/j.porgcoat.2008.08.010.
[34] J.X. Liu, D.Z. Yang, F. Shi, Y.J. Cai, Sol-gel deposited TiO2 film on NiTi surgical alloy for biocompatibility improvement, Thin Solid Films. 429 (2003) 225–230. https://doi.org/10.1016/S0040-6090(03)00146-9.
[35] M. Gerritsen, A. Kros, V. Sprakel, J.A. Lutterman, R.J.M. Nolte, J.A. Jansen, Biocompatibility evaluation of sol-gel coatings for subcutaneously implantable glucose sensors, Biomaterials. 21 (2000) 71–78. https://doi.org/10.1016/S0142-9612(99)00136-2.
[36] M. Manso, M. Langlet, J.M. Martínez-Duart, Testing sol-gel CaTiO3 coatings for biocompatible applications, Mater. Sci. Eng. C. 23 (2003) 447–450. https://doi.org/10.1016/S0928-4931(02)00319-3.
[37] J. Rams, A. Ureña, M.D. López, A.J. López, Characterisation of multilayered sol-gel silica coatings on aluminium-SiC composites, Surf. Coatings Technol. 201 (2006) 3715–3722. https://doi.org/10.1016/j.surfcoat.2006.09.004.
[38] M.L. Zheludkevich, I.M. Salvado, M.G.S. Ferreira, Sol-gel coatings for corrosion protection of metals, J. Mater. Chem. 15 (2005) 5099–5111. https://doi.org/10.1039/b419153f.
[39] L. Landau, B. Levich, Dragging of a Liquid by a Moving Plate, Acta Physicochim. URSS. 17 (1942) 42–54. https://doi.org/10.1016/b978-0-08-092523-3.50016-2.

[40] H.C. Mayer, R. Krechetnikov, Landau-Levich flow visualization: Revealing the flow topology responsible for the film thickening phenomena, Phys. Fluids. 24 (2012). https://doi.org/10.1063/1.4703924.
[41] R. Krechetnikov, G.M. Homsy, Experimental study of substrate roughness and surfactant effects on the Landau-Levich law, Phys. Fluids. 17 (2005). https://doi.org/10.1063/1.2112647.
[42] M. Mozammel, M. Khajeh, N.N. Ilkhechi, Effect of Surface Roughness of 316 L Stainless Steel Substrate on the Morphological and Super-Hydrophobic Property of TiO2 Thin Films Coatings, Silicon. 10 (2018) 2603–2607. https://doi.org/10.1007/s12633-018-9796-1.
[43] J. Krzak-Roś, J. Filipiak, C. Pezowicz, A. Baszczuk, M. Miller, M. Kowalski, R. Będziński, The effect of substrate roughness on the surface structure of TiO 2, SiO2, and doped thin films prepared by the sol-gel method, Acta Bioeng. Biomech. 11 (2009) 21–29.
[44] H. Zhao, M. Yu, J. Liu, S. Li, B. Xue, M. Liang, Effect of Surface Roughness on Corrosion Resistance of Sol-Gel Coatings on AA2024-T3 Alloy, J. Electrochem. Soc. 162 (2015) C718–C724. https://doi.org/10.1149/2.0271514jes.
[45] L. Ponsonnet, K. Reybier, N. Jaffrezic, V. Comte, C. Lagneau, M. Lissac, C. Martelet, Relationship between surface properties (roughness, wettability) of titanium and titanium alloys and cell behaviour, Mater. Sci. Eng. C. 23 (2003) 551–560. https://doi.org/10.1016/S0928-4931(03)00033-X.
[46] N. Pulido-González, S. García-Rodríguez, M. Campo, J. Rams, B. Torres, Application of DOE and ANOVA in Optimization of HVOF Spraying Parameters in the Development of New Ti Coatings, J. Therm. Spray Technol. 29 (2020) 384–399. https://doi.org/10.1007/s11666-020-00989-9.
[47] Z. Yoshimitsu, A. Nakajima, T. Watanabe, K. Hashimoto, Effects of surface structure on the hydrophobicity and sliding behavior of water droplets, Langmuir. 18 (2002) 5818–5822. https://doi.org/10.1021/la020088p.
[48] S.J. Hitchcock, N.T. Carroll, M.G. Nicholas, Some effects of substrate roughness on wettability, J. Mater. Sci. 16 (1981) 714–732. https://doi.org/10.1007/bf00552210.
[49] J. Bengourram, F. Hamadi, M. Mabrouki, N. Kouider, M. Zekraoui, M. Ellouali, H. Latrache, Relationship between roughness and physicochemical properties of glass surface and theoretical adhesion of bacterial cells, Phys. Chem. News. 47 (2009) 138–144.

Table I. AZ31B magnesium alloy composition in wt. %.

Al	Zn	Mn	Si	Ca	Fe	Ni	Cu	Mg
2.9	0.75	0.29	0.01	<0.005	0.004	0.0013	<0.0005	Bal.